JACS
JOURNAL OF THE AMERICAN CHEMICAL SOCIETY

Article

pubs.acs.org/JACS

Cell Protective, ABC Triblock Polymer-Based Thermoresponsive Hydrogels with ROS-Triggered Degradation and Drug Release

Mukesh K. Gupta,[†] John R. Martin,[†] Thomas A. Werfel,[†] Tianwei Shen,[†] Jonathan M. Page,[‡] and Craig L. Duvall*[,†]

[†]Biomedical Engineering, Vanderbilt University, Nashville, Tennessee 37235, United States

[‡]Chemical and Biomolecular Engineering, Vanderbilt University, Nashville, Tennessee 37235, United States

Supporting Information

ABSTRACT: A combination of anionic and RAFT polymerization was used to synthesize an ABC triblock polymer poly-[(propylenesulfide)-*block*-(*N*,*N*-dimethylacrylamide)-*block*-(*N*-isopropylacrylamide)] (PPS-*b*-PDMA-*b*-PNIPAAM) that forms physically cross-linked hydrogels when transitioned from ambient to physiologic temperature and that incorporates mechanisms for reactive oxygen species (ROS) triggered degradation and drug release. At ambient temperature (25 °C), PPS-*b*-PDMA-*b*-PNIPAAM assembled into 66 ± 32 nm micelles comprising a hydrophobic PPS core and PNIPAAM on the outer corona. Upon heating to physiologic temperature (37 °C), which exceeds the lower critical solution temperature (LCST) of PNIPAAM, micelle solutions (at ≥2.5 wt %) sharply transitioned into stable, hydrated gels. Temperature-dependent rheology indicated that the equilibrium storage moduli (G') of hydrogels at 2.5, 5.0, and 7.5 wt % were 20, 380, and 850 Pa, respectively. The PPS-*b*-PDMA-*b*-PNIPAAM micelles were preloaded with the model drug Nile red, and the resulting hydrogels demonstrated ROS-dependent drug release. Likewise, exposure to the peroxynitrite generator SIN-1 degraded the mechanical properties of the hydrogels. The hydrogels were cytocompatible *in vitro* and were demonstrated to have utility for cell encapsulation and delivery. These hydrogels also possessed inherent cell-protective properties and reduced ROS-mediated cellular death *in vitro*. Subcutaneously injected PPS-*b*-PDMA-*b*-PNIPAAM polymer solutions formed stable hydrogels that sustained local release of the model drug Nile red for 14 days *in vivo*. These collective data demonstrate the potential use of PPS-*b*-PDMA-*b*-PNIPAAM as an injectable, cyto-protective hydrogel that overcomes conventional PNIPAAM hydrogel limitations such as syneresis, lack of degradability, and lack of inherent drug loading and environmentally responsive release mechanisms.

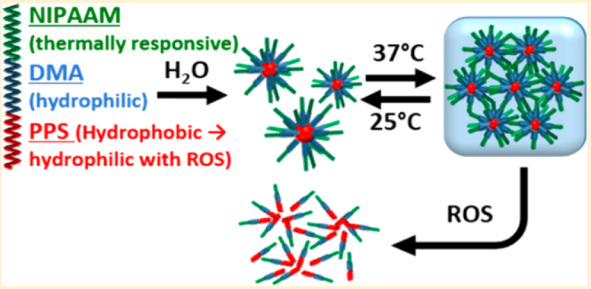

INTRODUCTION

Injectable, *in situ* forming biodegradable polymeric hydrogels that are responsive to environmental or externally applied stimuli (such as temperature, pH, ultrasonic sound, light, or ionic strength) provide promising platforms for encapsulation and delivery of drugs and/or cells in a variety of biomedical applications.[1−5] Poly(*N*-isopropylacrylamide) (PNIPAAM) has been extensively studied for drug[6,7] and cell delivery[8] applications because of its lower critical solution temperature (LCST) (at ∼32 °C)[6,7] that enables injection of solutions at ambient temperature that gel *in situ* at physiologic temperature. This overcomes practical manufacturing and storage issues related to prefabricated hydrogel/scaffold systems and avoids the need for potentially damaging ultraviolet irradiation or addition of cytotoxic reagents as required for many PEG-based systems that can be cross-linked *in situ*.[9,10] However, PNIPAAM homopolymers suffer from syneresis (hydrogel deswelling/hydrophobic collapse), lack of biodegradability, and absence of inherent mechanisms for drug loading and/or environmentally triggered release.[11,12] More recently, biodegradable variants of PNIPAAM have been reported,[13−22] though these second generation materials also lack mechanisms for drug loading and controlled, *in situ* release. Thus, there remains a significant, unmet need for hydrogels engineered to possess inherent degradation and sustained, "smart" drug release mechanisms that allow the biomedical community to more fully harness the full potential of thermo-reversible hydrogels for parenteral applications.

Recently, ABC triblock copolymer based micelles were reported for the formation of thermoresponsive hydrogels.[23−26] Polymers with ABC triblock architecture undergo sharp gelation at low polymer concentration, but this type of system has not been endowed with biodegradability or "smart" drug release mechanisms desirable for biomedical applications. Here, an ABC triblock polymer was utilized, for the first time, to form biodegradable thermo-gels amenable to cell and drug delivery. Furthermore, for the first time, a PNIPAAM-based thermogel was endowed with a reactive oxygen species (ROS)-responsive mechanism for degradation and drug release. This hydrogel

Received: July 25, 2014
Published: September 25, 2014

   dx.doi.org/10.1021/ja507626y | *J. Am. Chem. Soc.* 2014, 136, 14896−14902

comprised the well-defined, micelle-forming ABC triblock polymer poly[(propylenesulfide)-*block*-(*N*,*N*-dimethylacylamide)-*block*-(*N*-isopropylacrylamide)] (PPS_{60}-*b*-$PDMA_{150}$-*b*-$PNIPAAM_{150}$). Due to the hydrophobicity of the PPS "A" block, the polymer self-assembles at room temperature into micelles that can be preloaded with hydrophobic drugs prior to *in situ* gelation. Heating PPS_{60}-*b*-$PDMA_{150}$-*b*-$PNIPAAM_{150}$ solutions to above the LCST of the PNIPAAM "C" block (e.g., body temperature) triggers phase transition of PNIPAAM on the outer micelle corona from soluble to insoluble and induces supramolecular assembly into noncytotoxic, nonsyneresing hydrogels that remain hydrated due to the hydrophilic PDMA "B" block.[27,28] When exposed to ROS, PPS slowly undergoes a two-stage phase transition to more hydrophilic poly(propylene sulfoxide) and ultimately poly(propylene sulphone),[29] which in this system, triggers sustained, "on-demand" drug release and hydrogel degradation. We and others have previously utilized PPS to generate micelles and polymersomes that leverage this ROS-triggered phase change to trigger nanoparticle disassembly and "smart" drug release,[21,30,31] but to our knowledge, this represents the first application of PPS in hydrogel macro-biomaterials. This new hydrogel integrates thermoresponsive PNIPAAM with the emerging concept of utilizing ROS responsive materials for environmentally demanded drug delivery.[9,32−34] Using ROS as a trigger for degradation and/or drug release has strong potential for biomedical applications because upregulation of oxidative stress is associated with the development and progression of many pathologies, including arthritis, atherosclerosis, aging, diabetes, and cancer.[35,36]

RESULTS AND DISCUSSION

Polymer Synthesis and Characterization. Scheme 1 outlines the synthesis steps for preparation of the PPS_{60}-*b*-$PDMA_{150}$-*b*-$PNIPAAM_{150}$ triblock corpolymer. The first step involves anionic polymerization of propylene sulfide using 1-butanethiol as an initiator in the presence of 1,8-diazabicyclo[5.4.0]undec-7-ene (DBU) in tetrahydrofuran (THF) at 0 °C for 2 h. To form a PPS-based reversible addition−fragmentation chain-transfer (RAFT) macro chain transfer agent (CTA), the propagation of the PPS chain polymerization was quenched by the addition of 2-iodoethanol to introduce hydroxyl groups at one of the terminal ends of the PPS. The hydroxyl functionalization of PPS was confirmed by ^{1}H NMR spectroscopy based on the appearance of the CH_2 proton peak near to the terminal OH group at 3.75 ppm (Supporting Information Figure S1A).

Scheme 1. Synthesis of PPS_{60}-*b*-$PDMA_{150}$-*b*-$PNIPAAM_{150}$ Triblock Copolymer via Anionic and RAFT Polymerization

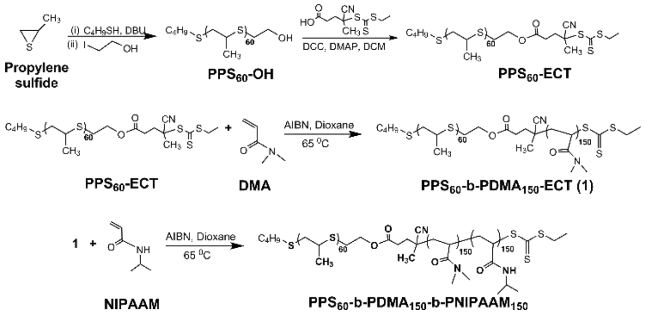

The terminal hydroxyl of PPS_{60}-OH was utilized to couple with the RAFT CTA 4-cyano-4-(ethylsulfanyltiocarbonyl) sulfanylpentanoic acid (ECT) using standard DCC/DMAP chemistry, as we have previously done to form a more standard PEG macro-CTA.[37] The conjugation of ECT to PPS_{60}-OH was confirmed by ^{1}H NMR based on the shift of the CH_2 proton peak from 3.75 to 4.2 ppm, which is characteristic of ester bond formation (Supporting Information Figure S1B). The ^{1}H NMR spectra of PPS_{60}-ECT showed an 81% conjugation of ECT onto PPS_{60}-OH as calculated from the ratio of the CH_2 proton peak at 3.4 ppm to the PPS methyl proton peak at 1.35 ppm. The PPS_{60}-ECT was then employed for the RAFT polymerization of DMA using AIBN in dioxane at 65 °C, for 24 h. The clear shift in the gel permeation chromatography (GPC) trace and the presence of characteristic PDMA peaks in the ^{1}H NMR spectra indicated the successful formation of the diblock copolymer (Supporting Information Figure S1C). At this point, any residual, unreacted PPS that was not coupled to ECT and chain extended with PDMA by RAFT was purified from the product by precipitation of the diblock copolymer into cold diethyl ether (which dissolves PPS but not PPS-PDMA). The PPS_{60}-*b*-$PDMA_{150}$ diblock macro-CTA was then utilized for triblock copolymerization of NIPAAM in dioxane at 65 °C using AIBN for 9 h (Supporting Information Figure S1D).

The GPC traces demonstrated a small, lower molecular weight shoulder on the triblock polymer (approximately 10% chain termination), but the molecular weights of each of the polymer blocks were relatively well-controlled and monodispersed (Figure 1, Table 1). These block lengths were chosen

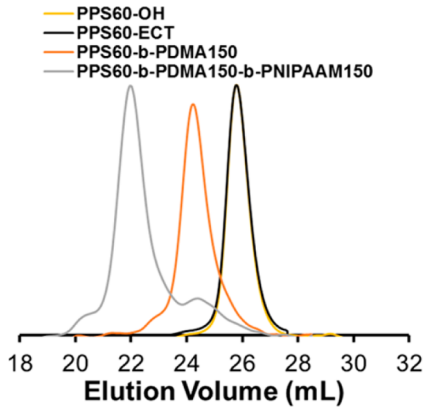

Figure 1. GPC refractive index detector traces of PPS_{60}-OH, PPS_{60}-ECT, PPS_{60}-*b*-$PDMA_{150}$, and PPS_{60}-*b*-$PDMA_{150}$-*b*-$PNIPAAM_{150}$ confirmed formation of the ABC polymer architecture.

Table 1. Molecular Weight Data for PPS_{60}-*b*-$PDMA_{150}$-*b*-$PNIPAAM_{150}$ at Each Step in the Synthesis

polymer	$M_{n,\ Th}$ [a]	$M_{n,\ NMR}$ [b]	$M_{n,\ GPC}$ [c]	PDI [d]
PPS_{60}-OH	4500	4445	4200	1.3
PPS_{60}-ECT	4762	4729	4500	1.3
PPS_{60}-*b*-$PDMA_{150}$	19762	20629	19800	1.1
PPS_{60}-*b*-$PDMA_{150}$-*b*-$PNIPAAM_{150}$	36712	37127	38800	1.3

[a]Theoretical molecular weight calculated based on monomer conversion. [b]Molecular weight based on ^{1}H NMR analysis. [c]Number-average absolute molecular weight determined by GPC equipped with refractive index and multiangle light scattering detectors. [d]Polydispersity index determined by GPC analysis.

dx.doi.org/10.1021/ja507626y | J. Am. Chem. Soc. 2014, 136, 14896−14902

based on a qualitative prescreening of a small library of polymers with varied lengths of the PDMA and PNIPAAM blocks. Qualitatively, it was observed that larger PDMA block length caused a small upward shift in the LCST toward physiological temperature and that smaller PNIPAAM blocks yielded materials that formed less mechanically robust hydrogels. PPS_{60}-*b*-$PDMA_{150}$-*b*-$PNIPAM_{150}$ became the focus of more in-depth studies based on having a desirable LCST value and robust hydrogel formation and stability in this prescreening.

Formation and Characterization of Polymer Micelles. The ABC triblock polymer design was sought because of its robust and rapid hydrogel formation and also because this architecture enables formation of stable core−shell structures in aqueous solutions at room temperature that can assemble into well-ordered 3D hydrogels once heated above the LCST of the PNIPAAM "C" block.[25] Assembly of the diblock PPS_{60}-*b*-$PDMA_{150}$ and triblock PPS_{60}-*b*-$PDMA_{150}$-*b*-$PNIPAAM_{150}$ polymers into micelles in aqueous media was confirmed by dynamic light scattering (DLS)-based size measurements. The DLS measurements of micelle size showed that the diblock and triblock polymer micelles at a 1 mg/mL concentration in DPBS (pH 7.4) at room temperature had an average diameter of 61 ± 30 nm and 66 ± 32 nm, respectively (Supporting Information Figure S2).

Preparation and Characterization of Hydrogels. The vial inversion method was next utilized to test the gelation behavior of aqueous PPS_{60}-*b*-$PDMA_{150}$-*b*-$PNIPAAM_{150}$ micelle solutions ranging from 2.0 to 7.5 wt % concentrations at 37 °C (Supporting Information Figure S3). It has been reported that ABC triblock polymers undergo a sharper gel transition and form hydrogels at lower polymer concentrations relative to randomly ordered ABA triblock copolymers.[23] In agreement with these observations, the PPS_{60}-*b*-$PDMA_{150}$-*b*-$PNIPAAM_{150}$ solutions transitioned into stable hydrogels within 30 s at and above 2.5 wt % concentration and returned to transparent solutions when cooled to ambient temperature. The gelling time was inversely related to the concentration of the polymer solutions. Hydrogel formation at 2.5 wt % is lower than most hydrogels and comparable to the best-performing, previously reported ABC triblock copolymers. Importantly, the gelation temperature of our system was physiologically relevant (between room and body temperature), which is an advantage over other previously reported ABC triblock polymer-based hydrogels that formed at 5 wt % but only once heated to above 37 °C.[23,25]

To further validate the architecture of the micelle structures at room temperature and their assembly into 3D networks at 37 °C, TEM samples of the polymer were prepared at 25 and 37 °C (Figure 2A). As shown in Figure 2B and Supporting Information Figure S4, PPS_{60}-*b*-$PDMA_{150}$-*b*-$PNIPAAM_{150}$ showed individual micellar structures at 25 °C. Consistent with other reports,[23] there was an increase in number and density of micelles and a more ordered structure for samples dried at 37 °C. For the first time, to our knowledge, STEM elemental mapping was utilized to image micelle structure and the apparent fusion of ABC polymer-based micelles through the PNIPAAM on the outer micelle corona upon heating to 37 °C. STEM element maps of sulfur (red, corresponding to the PPS) and of oxygen (green, corresponding to PDMA and PNIPAAM) on samples prepared at 37 °C enabled visualization of core−shell architecture and merging of individual micelles with maintenance of distinct PPS cores (Figure 2C).

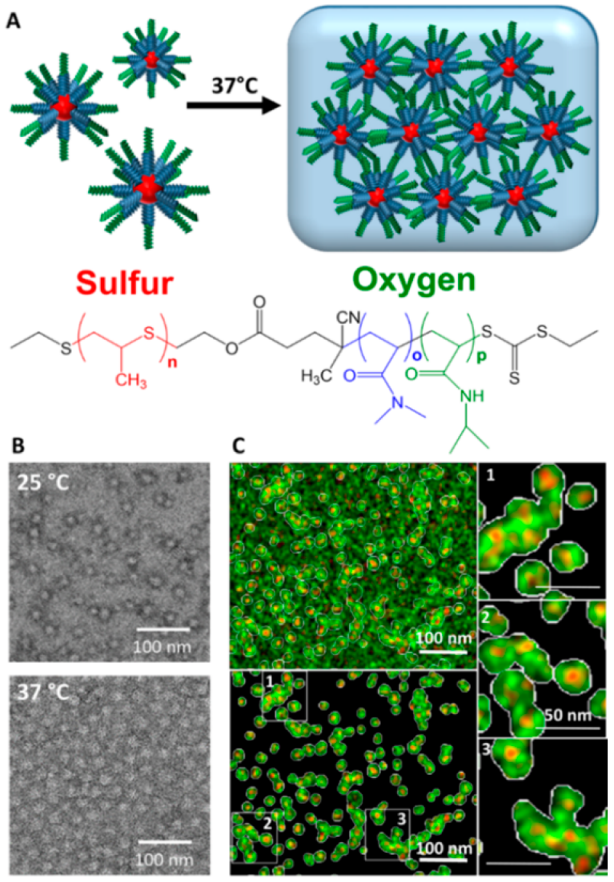

Figure 2. TEM/STEM-EDS confirmation of temperature dependent morphology switch. (A) Schematic representation of micelle gelation at 37 °C and polymer architecture coordinating with STEM-EDS element maps. (B) TEM images of PPS_{60}-*b*-$PDMA_{150}$-*b*-$PNIPAAM_{150}$ micelles at 25 and 37 °C. (C) STEM-EDS element maps for sulfur (red) and oxygen (green) of PPS_{60}-*b*-$PDMA_{150}$-*b*-$PNIPAAM_{150}$ core−shell compartments at 37 °C with image thresholding and background subtraction. Core-forming PPS produces the red signal for sulfur, while oxygen (appearing green) is present in the PDMA and PNIPAAM corona-forming blocks.

The LCST of the PPS_{60}-*b*-$PDMA_{150}$-*b*-$PNIPAAM_{150}$ micelles in an aqueous solution (1 wt % concentration) was determined by measuring the spectrophotometric absorption of polymer solutions while the temperature was ramped from 20 to 45 °C (Figure 3A). The polymer solutions exhibited a sharp change in absorption between 30 and 34 °C, which can be attributed to the well-known LCST of PNIPAAM near 32 °C.[6,7]

The LCST of NIPAAM-based random copolymers can be adjusted down or up by copolymerizing NIPAAM with hydrophobic and hydrophilic monomers, respectively.[38,39] The primary previous approach to forming degradable PNIPAAM hydrogels has involved copolymerization of hydrolytically degradable hydrophobic monomers that, once they degrade, shift the LCST to above body temperature and cause hydrogel dissolution.[16,20,33,40−43] However, this further complicates the synthesis because these degradable, hydrophobic monomers must be counterbalanced by copolymerization with another hydrophilic monomer in order to tune the initial LCST into a useful range between room and physiologic temperature. A strength of our well-defined ABC triblock architecture is that homopolymer PNIPAAM blocks constitute the surface of the preformed micelles, and these PNIPAAM segments are

dx.doi.org/10.1021/ja507626y | J. Am. Chem. Soc. 2014, 136, 14896−14902

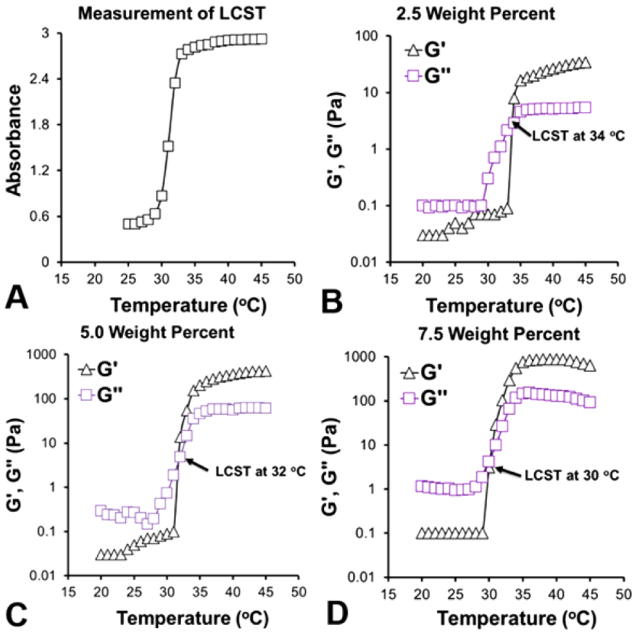

Figure 3. PPS_{60}-*b*-$PDMA_{150}$-*b*-$PNIPAAM_{150}$ gelation temperature and peak elastic modulus are dependent on concentration and are well-tuned for biomedical use. (A) LCST measurement of PPS_{60}-*b*-$PDMA_{150}$-*b*-$PNIPAAM_{150}$ at 1 wt % concentration in DPBS at pH 7.4 at 500 nm wavelength with a heating rate of 1 °C/min. (B–D) Measurement of storage (G') and loss moduli (G'') as a function of temperature for triblock copolymer solutions at (B) 2.5, (C) 5.0, and (D) 7.5 wt % with a heating rate of 1 °C/min at a frequency of 10 rad/s and 1% strain. The black arrows indicate the LCST value for each sample.

predominantly spatially isolated from the PPS and PDMA polymer blocks. Consequently, this ABC triblock copolymer demonstrated an LCST value similar to pure PNIPAAM homopolymers, allowing for thermo-reversible gelation at the biomedically useful temperature 32 °C.[39]

In addition to the STEM data in Figure 2C, the proposed polymer/micelle architecture is further supported by ^{1}H NMR spectra of the triblock copolymer in $CDCl_3$ and D_2O. The observation of each polymer block in these spectra is dependent on the solubility of each block in each solvent (Supporting Information Figure S1). In $CDCl_3$, all polymer blocks are well solvated, and the characteristic peaks from each polymer block were observed in the ^{1}H NMR spectrum (Supporting Information Figure S1D). In D_2O at 25 °C (Supporting Information Figure S1E), only peaks from the PDMA and PNIPAAM block were visible due to micelle assembly, driving the hydrophobic PPS into an insoluble core. At 37 °C, only peaks from the PDMA block were evident (Supporting Information Figure S1F) due to hydrophilic to hydrophobic transition of PNIPAAM above the LCST. These data further support formation of networks physically cross-linked through PNIPAAM and PPS hydrophobic domains separated by regions of hydrated PDMA.

Rheological Characterization of Hydrogels. Rheological analysis was performed to more quantitatively investigate the gelation temperature and mechanical properties of the PPS_{60}-*b*-$PDMA_{150}$-*b*-$PNIPAAM_{150}$ solutions at different polymer concentrations. Storage and loss moduli (G' and G'') were recorded during temperature sweeps from 20 to 45 °C with a heating rate of 1 °C/min at a frequency of 10 rad/s and a 1% strain. Figure 3B–D shows rheology data for 2.5, 5.0, and 7.5 wt % polymer solutions. The PPS_{60}-*b*-$PDMA_{150}$-*b*-$PNIPAAM_{150}$ solutions exhibited an increase in both G' and G'' when heated, and G' crossed over and exceeded G'' when the solutions gelled. The G' and G'' moduli values subsequently equilibrated while the solutions were heated beyond their LCSTs toward 37 °C. These data indicate that PPS_{60}-*b*-$PDMA_{150}$-*b*-$PNIPAAM_{150}$ forms stable hydrogels and highlights the potential utility of this system as an injectable therapeutic biomaterial that gels when exposed to physiologic temperature.

The gelation point (or rheological LCST) was defined as the cross over point between G' and G'', and these values were consistent with the UV-based LCST measurement (Figure 3A). The gelation points occurred at 34, 32, and 30 °C for the 2.5, 5.0, and 7.5 wt % polymer solutions, respectively, while a 10 wt % solution formed a viscous gel instead of a clear solution at room temperature. Gradual decrease in LCST with increasing polymer concentration was expected and is consistent with previously reported literature.[44] The equilibrium storage moduli (G') were dependent on polymer concentration and were 20, 380, and 850 Pa for 2.5, 5.0, and 7.5 wt % hydrogels, respectively (Figure 3B–D). These elastic moduli at each wt % were higher than values previously reported for ABC triblock copolymer hydrogels.[23,25] These data also suggest that hydrogel modulus can be tuned by varying the polymer concentration in order to tailor this system for specific applications. Furthermore, while many PNIPAAM-based hydrogels suffer from deswelling and collapse after being held at or above their LCST, the G' and G'' values of these hydrogels remained relatively stable after reaching 37 °C, indicating resistance to syneresis.[11] To verify that the polymer was within the linear viscoelastic region for the modulus and gelation experiments, frequency sweep measurements[23] were carried out on 5 wt % hydrogels in PBS over a 0.1–50 rad/s frequency sweep at 37 °C (Supporting Information Figure S5). At these frequencies, the polymer demonstrated linear solid like behavior.

Degradation of Hydrogels under ROS Environment. To determine the ROS-dependent degradation of the hydrogels, samples were placed in an accelerated oxidative environment with 0.5 M H_2O_2 (50–100 μM is considered physiologic[45]) at 37 °C (Figure 4A). After overnight exposure to these conditions, the polymer was no longer gelled at 37 °C,

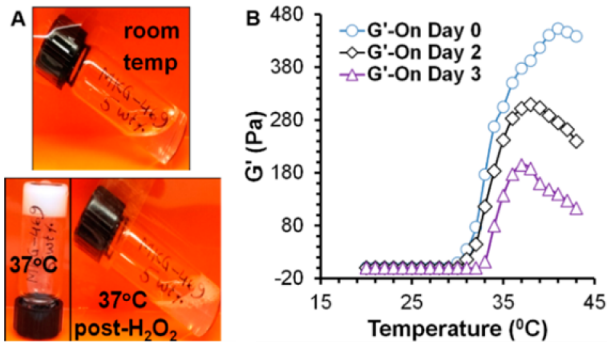

Figure 4. PPS_{60}-*b*-$PDMA_{150}$-*b*-$PNIPAAM_{150}$ hydrogels degrade under exposure to ROS. (A) The triblock polymer is soluble at room temperature, gels after 30 s at 37 °C, and is destabilized at 37 °C after overnight incubation with 0.5 M H_2O_2. (B) Measurement of storage (G') and loss modulus (G'') as a function of temperature for a 5 wt % polymer concentration after treatment with SIN-1 (1 mM) for varied amounts of time. Rheology data was gathered with a heating rate of 1 °C/min at a frequency of 10 rad/s and 1% strain.

dx.doi.org/10.1021/ja507626y | J. Am. Chem. Soc. 2014, 136, 14896–14902

providing proof of concept on the degradability of PPS_{60}-*b*-$PDMA_{150}$-*b*-$PNIPAAM_{150}$ hydrogels by ROS. To further investigate the ROS-dependent degradation mechanism of the PPS_{60}-*b*-$PDMA_{150}$-*b*-$PNIPAAM_{150}$ hydrogels, 3-morpholino-syndnomine (SIN-1) was used to model the continual production of ROS that would occur *in vivo*. SIN-1 decomposes into nitric oxide and superoxide, which combine to form the highly reactive oxidant peroxynitrite ($ONOO^-$).[46] A 1 mM SIN-1 concentration produces 10 μM peroxynitrite/min in PBS at pH 7.4.[47] Physiological concentrations of peroxynitrite *in vivo* have been estimated to be 50 μM,[48] and doses up to 1 mM SIN-1 are often utilized to deliver peroxynitrite (e.g., to mimic oxidative stress conditions) to cultured cells *in vitro*.[49−51]

ROS degradation of the mechanical strength of 5 wt % hydrogels was rheologically assessed on hydrogels exposed to 1 mM SIN-1. The G' values at 37 °C measured following 0, 2, or 3 days exposure to SIN-1 were 380, 300, and 200 Pa, respectively (Figure 4B). Thus, the presence of ROS-generating SIN-1 decreased the hydrogel elastic modulus over time, which can be attributed to an ROS-mediated oxidative transformation of PPS from hydrophobic to hydrophilic.[30] The 37 °C vial inversion method was used to assess hydrogel stability just prior to rheology measurement at each time point, and the hydrogels began to show visible instability on day 3. These conditions are useful in validating the ROS-dependent degradation mechanism of the hydrogels, but it is anticipated that the rate of degradation upon exposure to 1 mM SIN-1 (which is often used to mimic highly toxic levels of oxidative stress *in vitro*)[49,51] is accelerated relative to most *in vivo* environments. In pilot *in vivo* studies described below, the hydrogels have been qualitatively observed to be resorbed by 2−3 weeks following subcutaneous injection.

ROS-Mediated *in Vitro* Nile Red Release from Hydrogels. To assess *in vitro* drug release from the PPS_{60}-*b*-$PDMA_{150}$-*b*-$PNIPAAM_{150}$ hydrogels, Nile red (used as a model hydrophobic drug[52]) was encapsulated in micelles at room temperature. Nile red was utilized to track drug release because it is fluorescent when loaded into a hydrophobic environment but loses its fluorescence upon release into a polar (i.e., aqueous) environment. The Nile red-loaded micelles were formed into hydrogels by heating to 37 °C, and they were then incubated with H_2O_2 to mimic the presence of an accelerated pathophysiologic oxidative microenvironment.[53] Figure 5 shows the *in vitro*, H_2O_2-dependent drug release kinetics of Nile red-loaded hydrogels (5 wt %) incubated with H_2O_2 in PBS (1, 100, and 500 mM concentrations) at 37 °C over a 64 h time course. The fluorescence intensity of Nile red-loaded hydrogels treated with H_2O_2 decreased over time, and the rate of this decrease was dependent on the concentration of H_2O_2 present. As with the ROS-mediated physical degradation of the hydrogel, the decrease in Nile red fluorescence intensity under oxidative conditions can be explained by the oxidative phase transition of the PPS block from hydrophobic to hydrophilic.[30] These collective results confirm that PPS_{60}-*b*-$PDMA_{150}$-*b*-$PNIPAAM_{150}$ is amenable to drug loading and sustained, ROS-mediated release from *in situ*-formed hydrogels. Note that accelerated release conditions under supra-physiologic H_2O_2 doses were utilized in this study due to the need to leave the drug-loaded hydrogel samples within a plate reader maintained at 37 °C in order to take longitudinal measurements throughout the study.

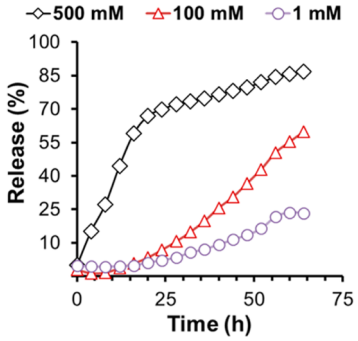

Figure 5. PPS_{60}-*b*-$PDMA_{150}$-*b*-$PNIPAAM_{150}$ hydrogels displays ROS concentration-dependent drug release. The *in vitro* H_2O_2-dependent drug release kinetics are shown for Nile red-loaded hydrogels (5 wt % triblock copolymer concentration) in PBS (pH 7.4) at 37 °C. To assess ROS-dependent drug release, hydrogel samples were incubated with 1, 100, and 500 mM H_2O_2 over a 64 h time course.

***In Vitro* Hydrogel Cytocompatibility and Protection against ROS Cytotoxicity.** Cytocompatibility of PPS_{60}-*b*-$PDMA_{150}$-*b*-$PNIPAAM_{150}$ hydrogels were tested by assessing viability of cells placed in direct contact with hydrogels. NIH 3T3 mouse fibroblasts were seeded in 2D and grown for 24 h before being overlaid with 5 wt % hydrogels, which were assessed after 4 and 24 h of additional culture. Viability of the adherent cells was evaluated with Live/Dead staining, qualitatively with fluorescent microscopy (Figure 6A) and

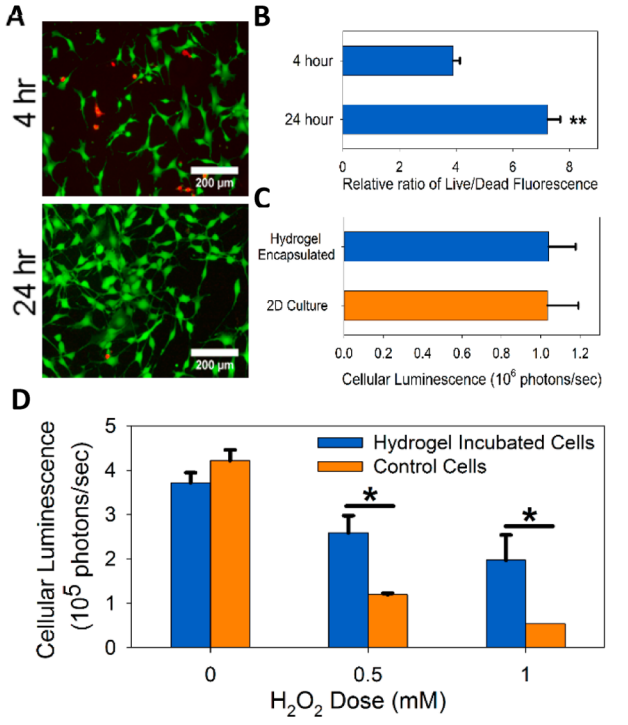

Figure 6. Cytocompatibility, cell encapsulation, and ROS protection with 5 wt % triblock copolymer hydrogels. (A) Microscopy images of cells stained with Calcein AM (live stain) and ethidium homodimer (dead stain) at 4 and 24 h after being overlaid with hydrogels. (B) Quantification of cellular fluorescence from Live/Dead staining, $^{**}p < 0.005$. (C) Demonstration of *in vitro* viability of NIH 3T3 mouse fibroblasts after 24 h of encapsulation within 5 wt % hydrogels. (D) Fibroblasts overlaid with hydrogels were protected from H_2O_2-induced cell death, demonstrating the inherent therapeutic capacity of these materials, $^{*}p < 0.05$.

dx.doi.org/10.1021/ja507626y | J. Am. Chem. Soc. 2014, 136, 14896−14902

quantitatively with microplate reader fluorescence measurements (Figure 6B). Both methods demonstrated high levels of cellular viability and proliferation over 24 h, supporting hydrogel cytocompatibility.

To further prove the utility of these polymers for potential use as cell delivery agents, NIH 3T3 mouse fibroblasts stably transduced to express luciferase were directly encapsulated into 5 wt % hydrogels, and relative cell number was measured based on luciferase activity over 24 h of culture (Figure 6C). Cell-generated bioluminescent signal 24 h postencapsulation was not significantly different from controls where cells were grown in 2D on tissue culture polystyrene (TCPS).

PPS is known to scavenge H_2O_2,[54] though to our knowledge, this inherent property has never been established to have therapeutic benefit. To explore whether PPS based hydrogels are cytoprotective against cytotoxic levels of H_2O_2, independent of loading with antioxidant or other therapeutics, luciferase-expressing fibroblasts were seeded in 2D culture and overlaid with 5 wt % hydrogels. Then, cells with and without hydrogels were incubated with varying doses of H_2O_2 for 24 h. After 24 h, the hydrogels were removed and the relative cell number quantified based on bioluminescence. In this context, the cytotoxic effects of H_2O_2 were significantly decreased in the presence of the hydrogels (Figure 6D). These results indicate that not only are these hydrogels cytocompatible but that they also serve as a sink for cytotoxic ROS, which is anticipated to be especially useful for enhancing efficacy of cell-based therapies.

***In Vivo* Drug Release from Subcutaneously Injected Hydrogels.** Finally, PPS_{60}-*b*-$PDMA_{150}$-*b*-$PNIPAAM_{150}$ hydrogels were applied in proof of concept *in vivo* studies for local delivery of the model hydrophobic drug Nile red. To demonstrate the sustained, local delivery of the drug from the hydrogels, 50 μL of dye-loaded triblock copolymer solution and dye-loaded diblock copolymer solution was injected subcutaneously in male BALB/c mice (Figure 7). For this study PPS_{60}-*b*-$PDMA_{150}$-*b*-$PNIPAAM_{150}$ and PPS_{60}-*b*-$PDMA_{150}$ micelles were preloaded with Nile red, which was imaged over time to determine local retention of the drug based on the controlled release hydrogels. The diblock polymer micelles were included as a control to confirm the utility of thermoresponsive gelation for local drug retention. The triblock polymer solutions formed robust hydrogels upon subcutaneous injection, while the diblock polymer solutions (not possessing the thermally responsive PNIPAAM block) were quickly dispersed from the injection site over 24 h (Figure 7A). The hydrogels showed local retention and release of the drug over 14 days (Figure 7B), verifying the utility of these hydrogels for sustained *in vivo* drug delivery.

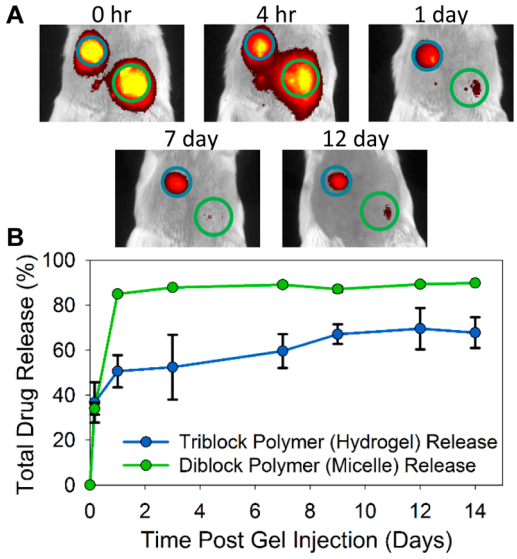

Figure 7. PPS_{60}-*b*-$PDMA_{150}$-*b*-$PNIPAAM_{150}$ hydrogels provide sustained, local drug release *in vivo*. (A) Representative images are shown from IVIS imaging to monitor local drug retention after subcutaneous injection of 50 μL of dye-loaded triblock polymer solution (blue circle, top left) and dye-loaded diblock copolymer solution (green circle, bottom right). The diblock copolymer micelles diffuse away rapidly, while the triblock copolymer solutions form robust hydrogels which retain and slowly release the model drug over 2 weeks. (B) Quantification of *in vivo* cumulative drug release from the drug-loaded triblock copolymer hydrogels and diblock micelles.

CONCLUSIONS

In summary, a novel, ROS-degradable, thermoresponsive ABC triblock polymer (PPS_{60}-*b*-$PDMA_{150}$-*b*-$PNIPAAM_{150}$) was synthesized with a well-controlled molecular weight by a combination of anionic and RAFT polymerization. In an aqueous solution at room temperature, the triblock polymer dissolved into a clear solution and assembled into stable micelles that, at relatively low concentrations, underwent sharp, reversible thermo-gelation when heated from room to physiologic temperature. The polymer gelation point was dependent on the concentration in solution, but a wide range of polymer concentrations showed gelation points within a biomedically relevant range. Temperature-dependent rheological characterization of PPS_{60}-*b*-$PDMA_{150}$-*b*-$PNIPAAM_{150}$ showcased its sharp, temperature-sensitive gelation and the lack of syneresis. ROS-dependent physical degradation of the hydrogels was demonstrated through exposure to ROS-producing SIN-1, along with the failure of hydrogels to reassemble after overnight incubation with H_2O_2. The triblock copolymer hydrogels also demonstrated a controlled, sustained, and ROS concentration-dependent release of the model drug Nile red. Crucially, the hydrogels exhibited minimal *in vitro* cytotoxicity with encapsulated fibroblasts while also demonstrating the ability to protect cells from H_2O_2-induced death. Finally, proof of concept *in vivo* studies demonstrated that subcutaneously injected triblock copolymer formed stable hydrogels that sustained local release of a model hydrophobic drug for at least 14 days. Collectively, these data demonstrate the potential utility of these new thermoresponsive triblock copolymers as an injectable, ROS-degradable platform for cell and drug delivery applications.

ASSOCIATED CONTENT

Supporting Information

The experimental details are provided. This material is available free of charge via the Internet at http://pubs.acs.org.

AUTHOR INFORMATION

Corresponding Author

craig.duvall@vanderbilt.edu

Notes

The authors declare no competing financial interest.

ACKNOWLEDGMENTS

This research was supported by the Vanderbilt University School of Engineering. Special thanks to Dr. Jeffrey Davidson and Fang Yu for guidance and assistance with designing and

implementing animal experiments. Tianwei Shen was supported by the Vanderbilt Undergraduate Summer Research Program (VUSRP). DLS, TEM (NSF EPS 1004083) and UV-based LCST measurements were conducted through the use of the core facilities of the Vanderbilt Institute of Nanoscale Sciences and Engineering (VINSE).

REFERENCES

(1) Nicodemus, G. D.; Bryant, S. J. *Tissue Eng., Part B* **2008**, *14*, 149.
(2) Li, Y.; Rodrigues, J.; Tomas, H. *Chem. Soc. Rev.* **2012**, *41*, 2193.
(3) Qiu, Y.; Park, K. *Adv. Drug Delivery Rev.* **2001**, *53*, 321.
(4) Yu, L.; Ding, J. *Chem. Soc. Rev.* **2008**, *37*, 1473.
(5) Hoffman, A. S. *Adv. Drug Delivery Rev.* **2002**, *54*, 3.
(6) Fujishige, S.; Kubota, K.; Ando, I. *J. Phys. Chem.* **1989**, *93*, 3311.
(7) Winnik, F. M. *Macromolecules* **1990**, *23*, 233.
(8) Ward, M. A.; Georgiou, T. K. *Polymers* **2011**, *3*, 1215.
(9) Lin, C.-C.; Anseth, K. *Pharm. Res.* **2009**, *26*, 631.
(10) Buwalda, S. J.; Boere, K. W. M.; Dijkstra, P. J.; Feijen, J.; Vermonden, T.; Hennink, W. E. *J. Controlled Release* **2014**, *190*, 254.
(11) Gan, T.; Guan, Y.; Zhang, Y. *J. Mater. Chem.* **2010**, *20*, 5937.
(12) Klouda, L.; Mikos, A. G. *Eur. J. Pharm. Biopharm.* **2008**, *68*, 34.
(13) Cui, Z.; Lee, B. H.; Pauken, C.; Vernon, B. L. *J. Biomed. Mater. Res.* **2011**, *98A*, 159.
(14) Wu, D.-Q.; Qiu, F.; Wang, T.; Jiang, X.-J.; Zhang, X.-Z.; Zhuo, R.-X. *ACS Appl. Mater. Interfaces* **2008**, *1*, 319.
(15) Huang, X.; Nayak, B. R.; Lowe, T. L. *J. Polym. Sci., Part A: Polym. Chem.* **2004**, *42*, 5054.
(16) Cui, Z.; Lee, B. H.; Vernon, B. L. *Biomacromolecules* **2007**, *8*, 1280.
(17) Wall, S. T.; Yeh, C.-C.; Tu, R. Y. K.; Mann, M. J.; Healy, K. E. *J. Biomed. Mater. Res.* **2010**, *95A*, 1055.
(18) Ekenseair, A. K.; Boere, K. W. M.; Tzouanas, S. N.; Vo, T. N.; Kasper, F. K.; Mikos, A. G. *Biomacromolecules* **2012**, *13*, 1908.
(19) Saito, T.; Fukai, A.; Mabuchi, A.; Ikeda, T.; Yano, F.; Ohba, S.; Nishida, N.; Akune, T.; Yoshimura, N.; Nakagawa, T.; Nakamura, K.; Tokunaga, K.; Chung, U.-i.; Kawaguchi, H. *Nat. Med.* **2010**, *16*, 678.
(20) Ma, Z.; Nelson, D. M.; Hong, Y.; Wagner, W. R. *Biomacromolecules* **2010**, *11*, 1873.
(21) Cerritelli, S.; ONeil, C. P.; Velluto, D.; Fontana, A.; Adrian, M.; Dubochet, J.; Hubbell, J. A. *Langmuir* **2009**, *25*, 11328.
(22) Vo, T. N.; Ekenseair, A. K.; Kasper, F. K.; Mikos, A. G. *Biomacromolecules* **2013**, *15*, 132.
(23) Zhou, C.; Hillmyer, M. A.; Lodge, T. P. *J. Am. Chem. Soc.* **2012**, *134*, 10365.
(24) Koonar, I.; Zhou, C.; Hillmyer, M. A.; Lodge, T. P.; Siegel, R. A. *Langmuir* **2012**, *28*, 17785.
(25) Li, C.; Buurma, N. J.; Haq, I.; Turner, C.; Armes, S. P.; Castelletto, V.; Hamley, I. W.; Lewis, A. L. *Langmuir* **2005**, *21*, 11026.
(26) Reinicke, S.; Schmelz, J.; Lapp, A.; Karg, M.; Hellweg, T.; Schmalz, H. *Soft Matter* **2009**, *5*, 2648.
(27) Kopeček, J.; Šprincl, L.; Bažilová, H.; Vacík, J. *J. Biomed. Mater. Res.* **1973**, *7*, 111.
(28) Šprincl, L.; Vacík, J.; Kopeček, J.; Lím, D. *J. Biomed. Mater. Res.* **1971**, *5*, 197.
(29) Napoli, A.; Valentini, M.; Tirelli, N.; Muller, M.; Hubbell, J. A. *Nat. Mater.* **2004**, *3*, 183.
(30) Gupta, M. K.; Meyer, T. A.; Nelson, C. E.; Duvall, C. L. *J. Controlled Release* **2012**, *162*, 591.
(31) Velluto, D.; Demurtas, D.; Hubbell, J. A. *Mol. Pharmaceutics* **2008**, *5*, 632.
(32) Lee, S. H.; Gupta, M. K.; Bang, J. B.; Bae, H.; Sung, H.-J. *Adv. Healthcare Mater.* **2013**, *2*, 908.
(33) Neradovic, D.; van Nostrum, C. F.; Hennink, W. E. *Macromolecules* **2001**, *34*, 7589.
(34) Huynh, C. T.; Nguyen, M. K.; Lee, D. S. *Macromolecules* **2011**, *44*, 6629.
(35) Winterbourn, C. C. *Nat. Chem. Biol.* **2008**, *4*, 278.
(36) Martin, J. R.; Gupta, M. K.; Page, J. M.; Yu, F.; Davidson, J. M.; Guelcher, S. A.; Duvall, C. L. *Biomaterials* **2014**, *35*, 3766.
(37) Nelson, C. E.; Kintzing, J. R.; Hanna, A.; Shannon, J. M.; Gupta, M. K.; Duvall, C. L. *ACS Nano* **2013**, *7*, 8870.
(38) Feil, H.; Bae, Y. H.; Feijen, J.; Kim, S. W. *Macromolecules* **1993**, *26*, 2496.
(39) Chung, J. E.; Yokoyama, M.; Aoyagi, T.; Sakurai, Y.; Okano, T. *J. Controlled Release* **1998**, *53*, 119.
(40) Neradovic, D.; van Steenbergen, M. J.; Vansteelant, L.; Meijer, Y. J.; van Nostrum, C. F.; Hennink, W. E. *Macromolecules* **2003**, *36*, 7491.
(41) Fujimoto, K. L.; Ma, Z.; Nelson, D. M.; Hashizume, R.; Guan, J.; Tobita, K.; Wagner, W. R. *Biomaterials* **2009**, *30*, 4357.
(42) Sun, L.-F.; Zhuo, R.-X.; Liu, Z.-L. *Macromol. Biosci.* **2003**, *3*, 725.
(43) Yoshida, T.; Aoyagi, T.; Kokufuta, E.; Okano, T. *J. Polym. Sci., Part A: Polym. Chem.* **2003**, *41*, 779.
(44) Lu, H.-F.; Targonsky, E. D.; Wheeler, M. B.; Cheng, Y.-L. *Biotechnol. Bioeng.* **2007**, *96*, 146.
(45) de Gracia Lux, C.; Joshi-Barr, S.; Nguyen, T.; Mahmoud, E.; Schopf, E.; Fomina, N.; Almutairi, A. *J. Am. Chem. Soc.* **2012**, *134*, 15758.
(46) Hogg, N.; Darley-Usmar, V. M.; Wilson, M. T.; Moncada, S. *Biochem. J.* **1992**, *281*, 419.
(47) Martin-Romero, F.; Gutiérrez-Martin, Y.; Henao, F.; Gutiérrez-Merino, C. *J. Fluoresc.* **2004**, *14*, 17.
(48) Mihm, M. J.; Bauer, J. A. *Biochimie* **2002**, *84*, 1013.
(49) Zhang, Y.; Wang, H.; Li, J.; Jimenez, D. A.; Levitan, E. S.; Aizenman, E.; Rosenberg, P. A. *J. Neurosci.* **2004**, *24*, 10616.
(50) Osna, N. A.; Haorah, J.; Krutik, V. M.; Donohue, T. M. *Hepatology* **2004**, *40*, 574.
(51) Zhang, Y.; Rosenberg, P. A. *Eur. J. Neurosci.* **2002**, *16*, 1015.
(52) Fowler, S. D.; Greenspan, P. *J. Histochem. Cytochem.* **1985**, *33*, 833.
(53) Seaver, L. C.; Imlay, J. A. *J. Biol. Chem.* **2004**, *279*, 48742.
(54) Hu, P.; Tirelli, N. *Bioconjugate Chem.* **2012**, *23*, 438.